CHEMISTRY OF MATERIALS

Article

pubs.acs.org/cm

Importance of Solubilizing Group and Backbone Planarity in Low Band Gap Polymers for High Performance Ambipolar field-effect Transistors

Joong Suk Lee,[†,⊗] Seon Kyoung Son,[‡,⊗] Sanghoon Song,[§] Hyunjung Kim,[§] Dong Ryoul Lee,[∥] Kyungkon Kim,[‡,⊥] Min Jae Ko,[‡] Dong Hoon Choi,[#] BongSoo Kim,*[,‡] and Jeong Ho Cho*[,¶]

[†]Department of Organic Materials and Fiber Engineering, Soongsil University, Seoul 156-743, Republic of Korea

[‡]Photo-electronic Hybrids Research Center, Korea Institute of Science and Technology (KIST), Seoul 136-791, Republic of Korea

[§]Department of Physics and Interdisciplinary Program of Integrated Biotechnology, Sogang University, Seoul 121-742, Republic of Korea

[∥]Department of Physics, Soongsil University, Seoul 156-743, Republic of Korea

[⊥]Department of Chemistry and Nano Science, Ewha Womans University, Seoul 156-743, Republic of Korea

[#]Department of Chemistry, Korea University, Seoul 136-713, Republic of Korea

[¶]SKKU Advanced Institute of Nanotechnology (SAINT) and Center for Human Interface Nano Technology (HINT), Department of Chemical Engineering, Sungkyunkwan University, Suwon 440-746, Republic of Korea

Supporting Information

ABSTRACT: We investigated the performance of ambipolar field-effect transistors based on a series of alternating low band gap polymers of oligothiophene and diketopyrrolopyrrole (DPP). The polymers contain oligothiophene units of terthiophene [T3] and thiophene-thienothiophene-thiophene [T2TT] and DPP units carrying branched alkyl chains of 2-hexyldecyl [HD] or 2-octyldodecyl [OD]. The structural variation allows us to do a systematic study on the relationship between the interchain stacking/ordering of semiconducting polymers and their resulting device performance. On the basis of synchrotron X-ray diffraction and atomic force microscopy measurements on polymer films, we found that longer branched alkyl side chains, i.e., OD, and longer and more planar oligothiophene, i.e., T2TT, generate the more crystalline structures. Upon thermal annealing, the crystallinity of the polymers was largely improved, and polymers containing a longer branched alkyl chain responded faster because longer alkyl chains have larger cohesive forces than shorter chains. For all the polymers, excellent ambipolar behavior was observed with a maximum hole and electron mobility of 2.2 and 0.2 $cm^2\ V^{-1}\ s^{-1}$, respectively.

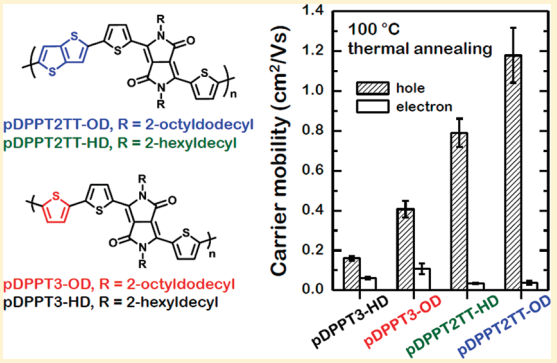

KEYWORDS: *polymer field-effect transistors, low band gap polymers, ambipolar transistors, crystalline structure, high carrier mobility*

1. INTRODUCTION

Organic semiconductors based on conjugated polymers are highly attractive for large-area low-cost electronic device applications, such as flexible displays, radiofrequency identification (RF-ID) tags, memory devices, and sensors.[1,2] Over the past decades, various conjugated polymers have been synthesized with the goal of improving the charge transport characteristics. Considerable progress has been made in developing p-type conjugated polymers.[3−6] Thiophene-based polymers, such as poly(3-hexylthiophene) (P3HT),[7] poly[5,5′-bis(3-dodecyl-2-thienyl)-2,2′-bithiophene)] (PQT),[8] and poly-(2,5-bis(3-alkylthiophene-2-yl)thieno[3,2-b]-thiophenes) (pBTTTs),[9] exhibited hole mobilities of 0.1−0.6 $cm^2V^{-1}\ s^{-1}$, and diketopyrrolopyrrole (DPP)-based polymers, such as PDQT,[10] P(DPP-alt-DTBSe),[11] and PDBT-co-TT[12] showed hole mobilities of 0.9−1.5 $cm^2\ V^{-1}\ s^{-1}$. Limited progress has been achieved in the context of n-type conjugated polymers.[1,13−15] For instance, ladder-type,[16,17] dithienodiimide-core,[18] and rylene dicarboximide-based polymers[19−22] have demonstrated electron mobilities of 0.001−0.1 $cm^2\ V^{-1}\ s^{-1}$. Recently, Yan et al. reported an electron mobility of 0.45−0.85 $cm^2\ V^{-1}\ s^{-1}$ for a naphthalene bis(dicarboximide)-based polymer, P(NDI2OD-T2).[23] In addition to the impressive mobility, they demonstrated fabrication of a polymeric complementary metal oxide semiconductor (CMOS)-like inverter using P3HT and P(NDI2OD-T2) as the p-channel and n-channel polymers, respectively.

Received: December 16, 2011
Revised: March 13, 2012
Published: March 14, 2012

CMOS devices that combine n-channel and p-channel semiconducting materials have low power dissipation requirements, a high noise tolerance margin, and excellent robustness.[2,13,24−28] For the construction of CMOS-like inverters, it is more desirable to use single-component ambipolar transistors than a combination of p- and n-channel transistors. The use of single-component transistors can simplify the design of circuits and minimize the number of device fabrication steps. In this regard, low band gap (typically, <1.5 eV) polymers with an alternating donor−acceptor structure are particularly suited for applications that require ambipolar transistors. The low energy offset between a metal's Fermi level and the frontier energy levels (i.e., the HOMO and LUMO) means that low band gap polymers have intrinsically low injection barriers for holes and electrons at the interface. However, low band gap polymer-based ambipolar transistors have not been systematically studied,[29−33] and the current state-of-the-art balanced hole and electron mobilities are 0.35 $cm^2\ V^{-1}\ s^{-1}$ and 0.40 $cm^2\ V^{-1}\ s^{-1}$, respectively.[30] To further advance the development of ambipolar polymer transistors, an in-depth investigation of the key factors that affect charge transport characteristics is required, including a study of the dependence of donor−acceptor structures on polymer chain stacking and orientation, the role of branched alkyl side chains, and the influence on transport of the alignment of a polymer's HOMO and LUMO with respect to the contact metal Fermi level.

In this study, we synthesized low band gap polymers based on oligothiophene-alt-DPP units with a systematic variation of oligothiophene units and branched side alkyl chain lengths. Synthetic routes are shown in Scheme 1. In synchrotron X-ray diffraction (XRD) and atomic force microscopy (AFM) measurements, we observed that longer branched alkyl side chains and longer interdistances between alkyl chains in the polymer backbone improve the crystalline structures in the polymer film. Moreover, thermal treatment stimulates the crystallinity in the polymer film. The polymer field-effect transistors (PFETs) showed excellent ambipolar behavior with high carrier mobilities of up to 2.2 and 0.2 $cm^2\ V^{-1}\ s^{-1}$, respectively. This work demonstrates that elaborate tuning of chemical structure and thermal annealing significantly modulate the interchain organization, which in turn affects the ambipolar PFET device performance.

Scheme 1. Synthesis of Oligothiophene-alt-DPP Polymers of pDPPT3-HD, pDPPT3-OD, pDPPT2TT-HD, and pDPPT2TT-OD

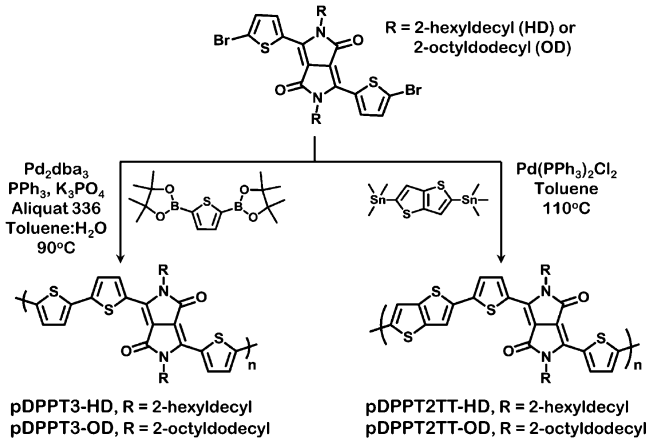

2. EXPERIMENTAL SECTION

2.1. Materials and Synthesis. Pd_2dba_3, $Pd(PPh_3)_2Cl_2$, Aliquat 336, *n*-BuLi (1.6 M in hexane), thiophene-2-carbonitrile, dibutyl succinate, and *N*-bromosuccinimide (NBS) were purchased from Sigma-Aldrich, Acros, and TCI. Common organic solvents were purchased from Daejung and J. T. Baker. Tetrahydrofuran (THF) was dried over sodium and benzophenone prior to use. All other reagents were used as received without further purification. The synthetic route and chemical structures of polymers used in this study are shown in Schemes 1 and 2. Compounds 1−8 were synthesized according to literature procedures.[18,32,34]

2.1.1. Synthesis of pDPPT3-HD. To a degassed 7 mL toluene solution of 2,5-bis(4,4,5,5-tetramethyl-1,3,2-dioxaborolan-2-yl)-thiophene (90 mg, 26.8 mmol), monomer 5 (0.242 g, 26.8 mmol), K_3PO_4 (0.284 g, 1.34 mmol), and three drops of Aliquat 336 was added 0.7 mL of degassed demineralized water. Pd_2dba_3 (9.8 mg, 0.0107 mmol) and triphenylphosphine (7.0 mg, 0.0268 mmol) were then added to the reaction mixture. The reaction solution was stirred for 1 h at 60 °C and 3 days at 90 °C under argon atmosphere. The reaction mixture was poured into methanol/HCl (6/1 v/v%) solution. The precipitated polymer was redissolved in chloroform and reprecipited in MeOH. The collected polymer was further purified by Soxhlet extraction using methanol, hexane, acetone, and chloroform. The chloroform fraction was collected and reprecipitated in methanol and filtered. The polymer was dried under vacuum, yielding 176 mg (79.3%). ^{1}H NMR ($CDCl_3$, 400 MHz) δ (ppm) 9.05 (b, 2H), 6.97 (b, 4H), 4.03 (b, 4H), 2.20 (b, 2H), 1.28−1.20 (b, 48 H), 0.89 (b, 12H). Anal. Calcd (%): C, 72.41; H, 8.75; N, 3.38; O, 3.86; S, 11.60. Found (%): C, 72; H, 8.7; N, 3.3; O, 4.1; S, 11.7. GPC M_n = 33 275; PDI = 2.83.

2.1.2. Synthesis of pDPPT3-OD. pDPPT3-OD was synthesized with the same method used for pDPPT3-HD, using 2,5-bis(4,4,5,5-tetramethyl-1,3,2-dioxaborolan-2-yl)thiophene (90 mg, 26.8 mmol) and monomer 7 (0.273 g, 26.8 mmol). The resulting polymer was obtained in 239 mg (94.7%). ^{1}H NMR ($CDCl_3$, 400 MHz) δ (ppm) 9.02 (b, 2H), 7.02 (b, 4H), 4.03 (b, 4H), 1.93 (b, 2H), 1.26−1.19 (b, 56 H), 0.84 (b, 12H). Anal. Calcd (%): C, 73.99; H, 9.42; N, 2.98; O, 3.40; S, 10.22. Found (%): C, 73.8; H, 9.5; N, 2.8; O, 3.4; S, 10.2. GPC M_n = 33 656; PDI = 6.08

2.1.3. Synthesis of pDPPT2TT-HD. Monomer 8 (200 mg, 42.9 mmol) and monomer 5 (388 mg, 42.9 mmol) were dissolved in degassed 7 mL of anhydrous toluene. Subsequently, a catalyst, $Pd(PPh_3)_2Cl_2$ (9.04 mg, 0.0129 mmol) was added into the reaction mixture and heated at 60 °C under argon atmosphere. After stirring for 1 h, the reaction solution was heated at 110 °C for 3 h under argon atmosphere. The reaction mixture was poured into methanol/HCl (6/1 v/v %) solution. The precipitated polymer was dissolved in chloroform, and the polymer was reprecipitated in methanol. The collected polymer was further purified by Soxhlet extraction using methanol, hexane, acetone, and chloroform. The chloroform fraction was collected and reprecipitated in methanol and filtered. The polymer was dried under vacuum, yielding 181 mg (60.0%). ^{1}H NMR ($CDCl_3$, 400 MHz) δ (ppm) 8.98 (b, 2H), 7.17 (b, 4H), 4.10 (b, 4H), 2.01 (b, 2H), 1.31−1.27 (b, 48 H), 0.91 (b, 12H). Anal. Calcd (%): C, 70.54; H, 8.20; N, 3.16; O, 3.61; S, 14.49. Found (%): C, 70.4; H, 8.3; N, 3.1; O, 3.39; S, 14.5. GPC M_n =20 657; PDI = 3.94.

2.1.4. Synthesis of pDPPT2TT-OD. pDPPT2TT-OD was synthesized with the same method used for pDPPT2TT-HD, using monomer 8 (200 mg, 42.9 mmol) and monomer 7 (0.438 g, 42.9 mmol) with a longer polymerization period of 3 days at 110 °C. The resulting polymer was obtained in 408 mg (95.0%). ^{1}H NMR ($CDCl_3$, 400 MHz) δ (ppm) 9.02 (b, 2H), 7.03 (b, 4H), 4.05 (b, 4H), 2.06 (b, 2H), 1.29−1.25 (b, 56 H), 0.89 (b, 12H). Anal. Calcd (%): C, 72.24; H, 8.89; N, 2.81; O, 3.21; S, 12.86. Found (%): C, 72.3; H, 8.7; N, 2.7; O, 3.3; S, 12.8. GPC M_n = 42 447; PDI = 4.34.

2.2. Material Characterization. ^{1}H NMR spectra were recorded on a Bruker advance 400 spectrometer (400 MHz). The molecular weights of polymers were measured by gel permeation chromatography (GPC) using chloroform as an eluent and polystyrene as a

Scheme 2. Synthesis of Monomers

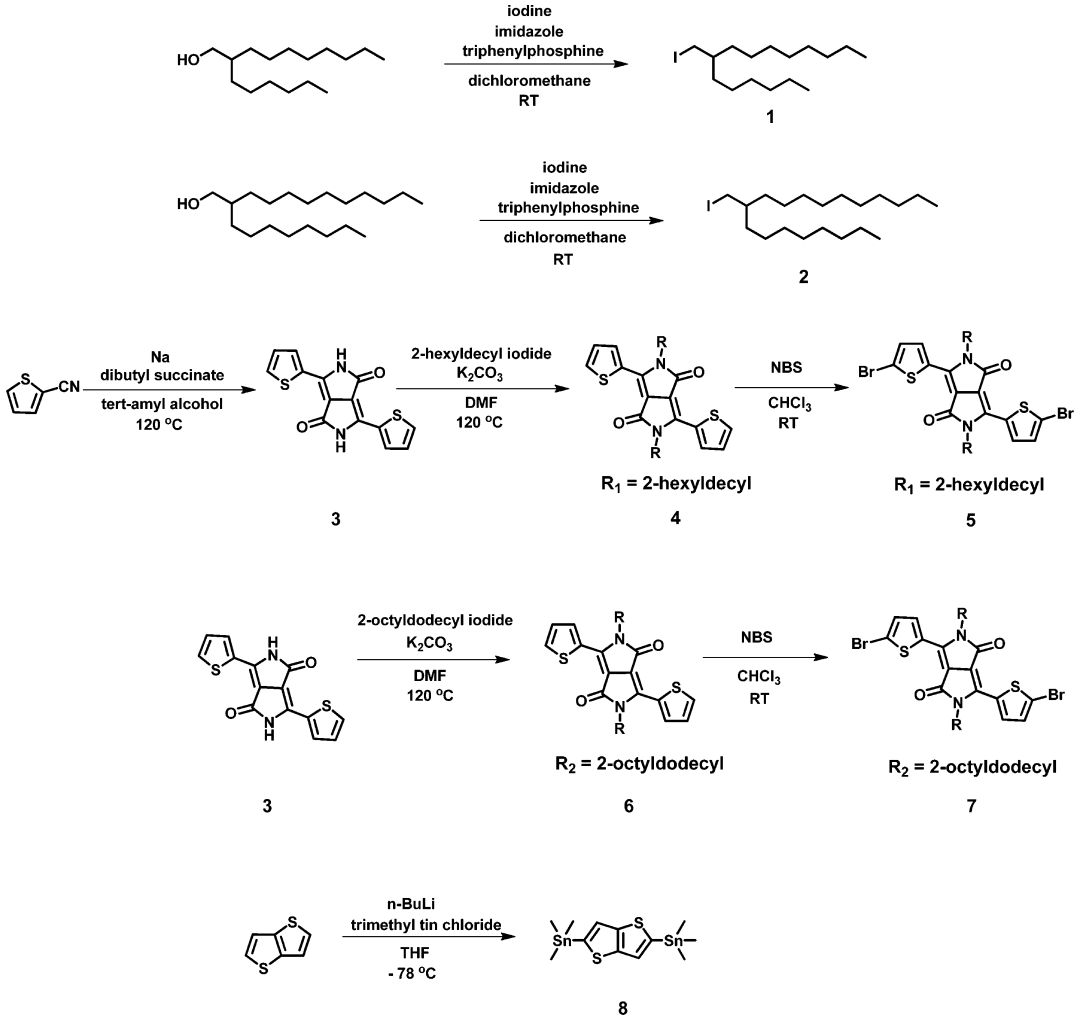

standard. Thermogravimetric analysis (TGA) was determined by a TA Q10 at a heating rate of 20 °C/min between 30 and 700 °C under nitrogen. Differential scanning calorimetry (DSC) was recorded on a Perkin-Elmer pyris 1 DSC instrument at a heating rate of 20 °C/min between 20 and 250 °C under nitrogen. UV−visible spectra were taken on a Perkin-Elmer Lamb 9 UV−vis spectrophotometer. Cyclic voltammetry (CV) was performed using a CH instruments electrochemical analyzer and solutions in degassed acetonitrile solution containing 0.1 M tetrabutylammonium hexafluorophosphate ($TBAPF_6$) as the electrolyte. The scan rate was 50 mV/s. A Pt wire electrode coated with a thin film of the polymer was used as the working electrode, a Pt wire was the counter electrode, Ag/Ag^+ was the reference electrode, and ferrocene was used as the internal standard. The crystalline structure of the ambipolar polymer films was characterized by synchrotron XRD studies at the 8-ID-E beamline of the Advanced Photon Source (APS) at Argonne. Surface morphology of the samples was investigated by a tapping mode AFM (D3100 Nanoscope V, Veeco). Transistor current−voltage characteristics were measured using Keithley 2400 and 236 source/measure units at room temperature under vacuum conditions (10^{-5} Torr) in a dark environment.

2.3. Device Fabrication. PFETs were fabricated on a highly doped n-type Si wafer with a thermally grown 300 nm thick oxide layer as the substrate. The wafer served as the gate electrode, whereas the thermally grown 300 nm thick SiO_2 layer acted as a gate insulator. Prior to treating the silicon oxide surface, the wafer was cleaned in piranha solution for 30 min at 100 °C and washed with copious amounts of distilled water. A SiO_2 layer was modified using an octadecyltrichlorosilane (ODTS, Gelest, Inc.) to reduce electron trapping by the silanol groups on SiO_2. A 40 nm thick layer of the ambipolar semiconducting polymer was spin-coated from a 0.5 wt % chloroform solution onto the ODTS-treated substrates. After spin-coating, the samples were dried in a vacuum chamber for 24 h. The ambipolar polymer films were thermally annealed for 30 min in a vacuum chamber at various temperatures, 25 °C, 100 °C, and 150 °C. The devices were completed by evaporating Au through a shadow mask to define the source and drain contact electrodes on the polymer film, with the channel length and width of 100 and 800 μm, respectively.

3. RESULTS AND DISCUSSION

We synthesized four low band gap oligothiophene-alt-DPP ambipolar semiconductors (pDPPT3-HD, pDPPT3-OD, pDPPT2TT-HD, and pDPPT2TT-OD where T stands for thiophene, TT [3,2-b]thienothiophene, HD 2-hexyldecyl, and OD 2-octyldodecyl) as shown in Schemes 1 and 2. UV−visible absorption spectroscopy (UV−visible) and cyclic voltammetry (CV) data showed that all the polymers yielded very low optical band gaps of 1.2−1.3 eV, and their HOMO and LUMO levels were −5.3 ∼ −5.5 eV and −3.9 ∼ −4.3 eV, respectively. The HOMO levels of pDPPT3-HD, pDPPT3-OD, and pDPPT2TT-HD are nearly the same (ca. −5.3 eV) within experimental errors, whereas that of pDPPT2TT-OD is slightly lower (−5.5 eV). The exceptionally high crystallinity of pDPPT2TT-OD in film (see below) and its longer alkyl chain induce the HOMO level

dx.doi.org/10.1021/cm2037487 | Chem. Mater. 2012, 24, 1316−1323

Table 1. Redox Potentials, Energy Levels, and Thermal Properties

	$E_{onset,ox}$ (V)	$E_{onset,red}$ (V)	HOMO[a] (eV)	LUMO[b] (eV)	$E_{g,opt}$[c] (eV)	T_d[d] (°C)
pDPPT3-HD	0.5	−1.40	−5.3	−4.0	1.3	387
pDPPT3-OD	0.5	−1.40	−5.3	−4.0	1.3	412
pDPPT2TT-HD	0.5		−5.3	−4.0	1.3	404
pDPPT2TT-OD	0.7		−5.5	−4.3	1.2	415

[a]HOMO = $E_{onset,ox}$ + 4.8 eV. [b]LUMO = HOMO − $E_{g,opt}$. [c]$E_{g,opt}$ was determined from the absorption onset of UV−vis spectra. [d]T_d was determined from the 5% weight-loss temperature under nitrogen.

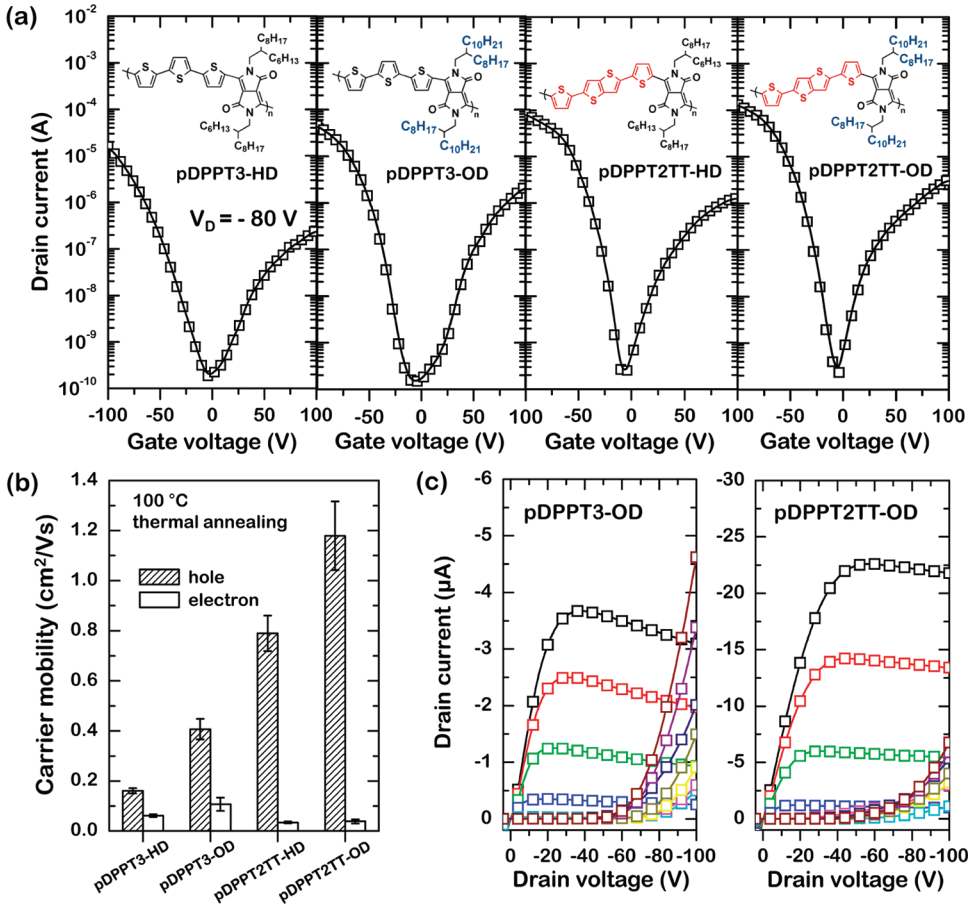

Figure 1. (a) Transfer characteristics at a fixed V_D of −80 V for PFETs based on ambipolar pDPPT3-HD, pDPPT3-OD, pDPPT2TT-HD, and pDPPT2TT-OD films annealed at 100 °C. (b) Hole and electron mobilities of all four polymer devices. (c) Output characteristics of PFETs based on pDPPT3-OD and pDPPT2TT-OD films annealed at 100 °C. The gate voltage was varied between −100 and 100 V in steps of −20 V.

lowering, which is consistent with previous reports.[35−38] Thermal analysis was performed using differential scanning calorimetry (DSC) and thermal gravimetric analysis (TGA). None of the polymers displayed a glass transition temperature (T_g) or melting temperature (T_m) over the range 30−250 °C, and the decomposition temperatures (T_d) were observed in the range 387−415 °C. All data demonstrated that the polymers were suitable for ambipolar transistor applications. The UV−visible, CV, DSC, and TGA data are summarized in Table 1 and those spectra are provided in Figure S1−S4 of the Supporting Information as well.

The performances of polymer field-effect transistors (PFETs) were investigated using a bottom-gate, top-contact configuration. Specifically, PFETs were built on heavily doped n-type Si substrates, which are commonly employed as gate electrodes. A thermally grown 300 nm thick SiO_2 layer served as the gate dielectric, and this layer was modified by functionalizing with octadecyltrichlorosilane (ODTS) to reduce charge trapping by the silanol groups on the SiO_2. A 40 nm thick ambipolar semiconducting film was spin-coated from a 0.5 wt % chloroform solution onto the ODTS-treated substrates. The spin-coated semiconducting polymers were thermally treated under vacuum at various annealing temperatures, including 25 °C, 100 °C, and 150 °C for 30 min. The 50 nm Au source/drain electrodes were thermally evaporated through shadow masks.

Figure 1a shows the transfer characteristics (drain current (I_D) vs gate voltage (V_G)) at a fixed drain voltage (V_D) of −80 V for PFETs based on pDPPT3-HD, pDPPT3-OD, pDPPT2TT-HD, and pDPPT2TT-OD films annealed at 100 °C. Clear V-shape ambipolar behavior was observed in hole-enhancement (V_D = −80 V) and electron-enhancement (V_D = +80 V) mode operations (Figures 1a and S5, Supporting Information). The hole and electron mobilities of each PFET were calculated in the respective saturation regimes using the relationship $I_D = C_i\mu W(V_G - V_{th})^2/2L$, where W and L are the

dx.doi.org/10.1021/cm2037487 | Chem. Mater. 2012, 24, 1316−1323

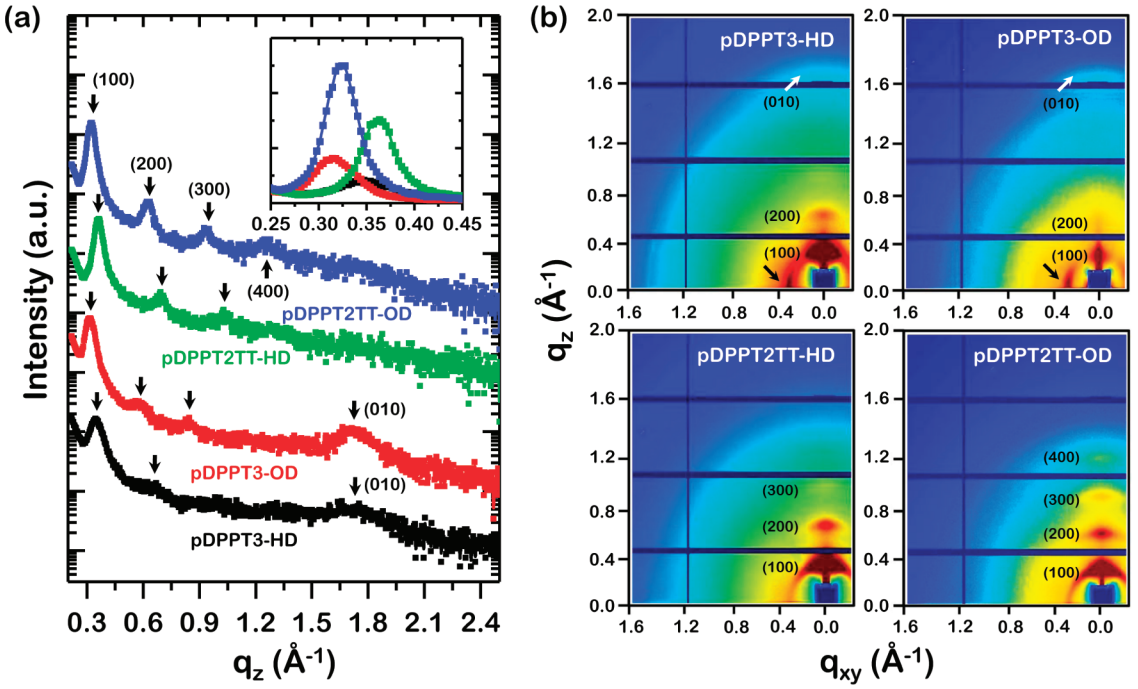

Figure 2. (a) XRD patterns and (b) 2D GIXD patterns of the pDPPT3-HD, pDPPT3-OD, pDPPT2TT-HD, and pDPPT2TT-OD films annealed at 100 °C.

channel width (800 μm) and length (100 μm), respectively, C_i is the specific capacitance of the gate dielectric (11 nF/cm^2), and μ is the carrier mobility. The PFETs based on pDPPT3-HD showed hole and electron mobilities of 0.16 and 0.06 cm^2 V^{-1} s^{-1}, respectively. Note that these mobilities were higher than values previously reported for devices fabricated on hexamethyldisilazane (HMDS)-treated surfaces (hole and electron mobilities of 0.04 and 0.01 cm^2 V^{-1} s^{-1}, respectively).[32] This difference is attributed to the more hydrophobic ODTS surface, which facilitated crystallization of the polymer. The PFETs based on pDPPT3-OD with longer alkyl side chains yielded PFETs with higher hole and electron mobilities of 0.41 and 0.11 cm^2 V^{-1} s^{-1}. The alkyl chain length dependence was also observed in the pDPPT2TT PFETs. These enhanced mobilities were related to the enhanced crystallization of polymers, which was confirmed by XRD and AFM studies (see below). Interestingly, pDPPT2TT PFETs exhibited much higher hole mobilities and slightly lower electron mobilities than pDPPT3 PFETs (see Figure 1b). The asymmetry between the hole and electron conduction can be ascribed to the density of the carrier hopping sites, i.e., a higher portion of donor units and a lower portion of acceptor units for a given volume.[33] The electrical properties of PFETs based on the polymers are summarized in Figure 1b. Figure 1c shows the output characteristics (I_D vs V_D) at 11 different V_Gs for PFETs based on pDPPT3-OD and pDPPT2TT-OD. The decrease in V_G from −100 to −20 V reduced the hole accumulation in the semiconducting channel, which then decreased I_D. In contrast, an increase in V_G from 0 to 100 V was accompanied by a gradual increase in I_D due to electron accumulation. The maximum I_D for the pDPPT2TT-OD PFETs in the hole saturation regime (V_D = −80 V) was much higher than that of the pDPPT3-OD PFETs.

The crystallinity and molecular orientation of the ambipolar semiconductor films, which influenced the carrier mobility, were characterized by synchrotron XRD. Figure 2a,b show, respectively, the XRD intensities measured along the surface normal direction and the 2D grazing incidence X-ray diffraction (2D GIXD) patterns. The surface-normal diffraction patterns in Figure 2a showed that the crystalline domains were oriented in one of two configurations with respect to the substrate: strong (100) reflections were due to a lamellar layer structure, and weak (010) reflections were due to π−π interchain stacking (spacing ≈ 3.65 Å), which indicated that the alkyl side chains were approximately aligned along the normal to the substrate, and the backbone was essentially parallel to the substrate. This molecular orientation was particularly favorable for charge transport through the π−π stacks in the PFETs, such that the drain current flowed along the semiconducting channel parallel to the substrate. The out-of-plane spacings of the ordered pDPPT3-HD, pDPPT3-OD, pDPPT2TT-HD, and pDPPT2TT-OD phases were calculated to be 18.1, 20.0, 17.3, and 19.4 Å, respectively. A comparison of these spacings to the fully extended polymer widths, i.e., two alkyl side chain lengths plus the aromatic backbone width, suggested that the side chains of the polymer were interdigitated and/or tilted out of the polymer backbone plane.

The (100) diffraction peak intensity was much more pronounced for the pDPPT2TT films than for the pDPPT3 films, and higher order diffraction peaks were observed. The pDPPT2TT produced only (100) reflections, whereas both (100) and (010) reflections were observed for the pDPPT3 films. The higher crystallinity in the pDPPT2TT films reflected the importance of the spacing between the alkyl chains. Longer TT groups provided more room for interdigitation/packing of the branched alkyl side chains and more efficient space filling, which in turn facilitated the long-range intermolecular organization and crystallization of the polymers. This argument was supported by the fact that the lamellar spacing was shorter for the pDPPT2TT polymers than for the corresponding pDPPT3 polymers and previous studies on poly(alkylthiophene)s.[8,9,39] The TT moieties also promoted cofacial interactions between the polymer backbones because the TT group presented a fused planar thiophene ring system, which enhanced the

dx.doi.org/10.1021/cm2037487 | Chem. Mater. 2012, 24, 1316−1323

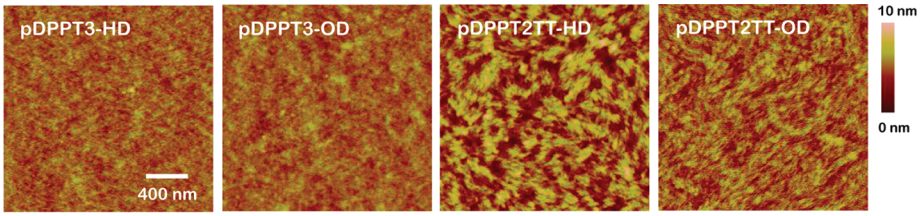

Figure 3. AFM images of the pDPPT3-HD, pDPPT3-OD, pDPPT2TT-HD, and pDPPT2TT-OD films annealed at 100 °C.

planarity of the polymer backbone. The higher diffraction peak intensity and the presence of higher order diffraction peaks in the polymers substituted with longer alkyl side chains suggested that the longer alkyl chains, i.e., OD, enhanced the crystallinity of the oligothiophene-alt-DPP semiconductors. The film crystallinity increased in the following order: pDPPT3-HD, pDPPT3-OD, pDPPT2TT-HD, and pDPPT2TT-OD (the inset of Figure 2a). This ordering was consistent with that of the device hole mobility, shown in Figure 1b. Overall, these results demonstrate that the interplay between the spacing between branched alkyl chains, the coplanarity, and the branched alkyl chain length affect significantly the degree of crystalline order in the ambipolar semiconductor films and the carrier mobility.

The crystallinity of each ambipolar semiconductor film was examined with greater precision by synchrotron GIXD measurements. Figure 2b shows the crystal reflections of the 2D GIXD patterns of the ambipolar semiconductor films annealed at 100 °C. The orientations of the ordered domains with respect to the substrate were similar among all four samples, specifically, the (100) peaks were found along the q_z axis perpendicular to the substrate, which optimized intermolecular $\pi-\pi$ stacking for efficient charge transport. However, the 2D GIXD pattern for the pDPPT3 films also exhibited a face-on orientation in which the (100) peaks appeared along the q_{xy} axis direction parallel to the substrate. Furthermore, highly scattered diffuse intensities around the (100) diffraction peaks along the Debye rings suggested that the deposited semiconductor films included crystal mismatches and dislocations in the vertical and lateral directions. pDPPT3-HD that includes shorter alkyl side chains displayed much stronger diffuse scattering intensities around the (100) diffraction peaks compared to the pDPPT3-OD that includes longer alkyl side chains. Similar results were observed in the pDPPT2TT films. AFM images of the ambipolar semiconductor films annealed at 100 °C are shown in Figure 3. The pDPPT3 films displayed aggregated granular surfaces, whereas the topography of the pDPPT2TT films exhibited highly developed crystalline fibrous structures, consistent with the XRD results.

Thermal annealing of the ambipolar semiconductors was found to affect the electrical properties of the devices. The representative transfer characteristics of PFETs based on ambipolar semiconducting polymer films annealed at various temperatures, namely, 25 °C, 100 °C, and 150 °C are shown in Figure S6, Supporting Information. The dependence of the hole and electron mobilities on the annealing temperature is summarized in Figure 4a and Table 2. Moreover, the changes in the crystalline structure and morphology were monitored by the X-ray diffraction patterns of the $\theta-2\theta$ scans and AFM measurements for four semiconducting films annealed at various substrate temperatures as shown in Figures 4b,d and S7, Supporting Information.

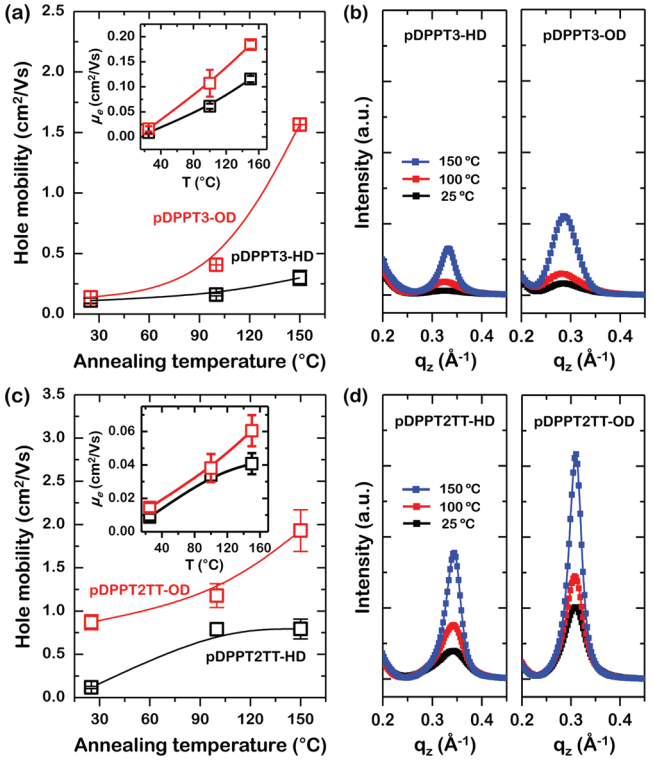

Figure 4. (a) Hole mobilities of PFETs based on ambipolar pDPPT3-HD and pDPPT3-OD films as a function of the annealing temperature. The inset shows the changes in the electron mobility. (b) The enlarged (100) Bragg peaks of the XRD pattern of pDPPT3-HD and pDPPT3-OD films. (c) Hole mobilities of PFETs based on ambipolar pDPPT2TT-HD and pDPPT2TT-OD films as a function of the annealing temperature. The inset shows the changes in the electron mobility. (d) The enlarged (100) Bragg peaks of the XRD pattern of pDPPT2TT-HD and pDPPT2TT-OD films.

Table 2. Hole and Electron Mobilities of PFETs Based on the Ambipolar pDPPT3-HD, pDPPT3-OD, pDPPT2TT-HD, and pDPPT2TT-OD Annealed at 25, 100, and 150 °C

		25 °C	100 °C	150 °C
pDPPT3-HD	hole	0.11 (±0.02)	0.16 (±0.01)	0.30 (±0.06)
	electron	0.01 (±0.001)	0.06 (±0.01)	0.12 (±0.01)
pDPPT3-OD	hole	0.14 (±0.01)	0.41 (±0.04)	1.57 (±0.16)
	electron	0.02 (±0.01)	0.11 (±0.03)	0.18 (±0.01)
pDPPT2TT-HD	hole	0.12 (±0.01)	0.79 (±0.07)	0.79 (±0.11)
	electron	0.01 (±0.002)	0.03 (±0.003)	0.04 (±0.01)
pDPPT2TT-OD	hole	0.87 (±0.09)	1.18 (±0.14)	1.93 (±0.24)
	electron	0.01 (±0.003)	0.04 (±0.01)	0.06 (±0.01)

Several important observations were made. First, the carrier mobility improves for higher annealing temperatures in all four

dx.doi.org/10.1021/cm2037487 | Chem. Mater. 2012, 24, 1316–1323

polymer devices. For instance, the hole mobility of pDPPT3-HD without thermal annealing was 0.11 $cm^2 V^{-1} s^{-1}$. Annealing of the polymer films at 100 and 150 °C resulted in an increase in the hole mobility to 0.16 and 0.30 $cm^2 V^{-1} s^{-1}$, respectively. This trend is well correlated with the (100) diffraction peak intensity that increased with the annealing temperature. The increase in the XRD peak intensity upon thermal annealing was due to a combination of the reorganization of the semiconducting polymers during heating and the growth of existing crystalline regions. This was confirmed by AFM experiments (Figures S7 and S8, Supporting Information). Therefore, we concluded that the observed enhancement in carrier mobility upon thermal annealing was due to more efficient $\pi-\pi$ stacking and greater intermolecular ordering. Note that there was no mobility improvement between 100 and 150 °C annealing while increasing the crystallinity for the pDPPT2TT-HD (Figure 4c). The relatively high roughness of pDPPT2TT-HD compared to the rest of the polymers (Figure S8, Supporting Information), which would lead to a poorer metal/polymer interface, may be responsible for this unexpected behavior. Second, a more sensitive dependence of crystallinity on the annealing temperature was observed for the ambipolar semiconductors substituted with longer alkyl side chains (Figure 4b,d). The alkyl side chains tend to move with thermal energy to maximize the van der Waals interactions. Because longer alkyl chains have larger cohesive forces than shorter chains, they responded faster to thermal annealing.[40,41] At the same time, the polymer main chains aligned with one another, which enhanced the overall crystallization of the polymers. Moreover, the hole mobility of pDPPT3-OD showed a sharper increase than that of pDPPT2TT-OD with the annealing temperature because the crystallinity of the pDPPT3-OD improved to a larger extent. Lastly, it should be noted that the highest hole mobility of 2.2 $cm^2 V^{-1} s^{-1}$ (average, 1.9 $cm^2 V^{-1} s^{-1}$) was achieved using the pDPPT2TT-OD annealed at 150 °C. An excellent hole mobility of 0.87 $cm^2 V^{-1} s^{-1}$ was measured without thermal treatment. These films may not require time-consuming annealing processes, which would be desirable for the high-throughput roll-to-roll mass production of PFET arrays.

4. CONCLUSIONS

In conclusion, we report the synthesis and characterization of low band gap polymers based on oligothiophene-alt-DPP polymers with two different oligothiophene and alkyl chain lengths. XRD patterns and AFM surface morphology images showed that longer branched alkyl side chains and longer interdistances between alkyl chains in the polymer improved the crystalline structures, which improved even further upon thermal annealing. Among the polymer field-effect transistors, excellent ambipolar transistor behavior was observed with very high hole and electron mobilities of up to 2.2 and 0.2 $cm^2 V^{-1} s^{-1}$, respectively. The hole mobilities were directly correlated with the crystalline structure and surface morphology of the polymer films. Overall, this work demonstrates the interdependence of the chemical structure, crystallinity, and carrier mobility, and provides a rational structure design approach to the fabrication of high-performance ambipolar PFETs.

■ ASSOCIATED CONTENT

Supporting Information

TGA thermograms, DSC curves, UV−vis absorption spectra, cyclic voltammetry curves, transfer characteristics of PFETs, AFM images, and RMS roughness as a function of annealing temperatuer. This material is available free of charge via the Internet at http://pubs.acs.org.

■ AUTHOR INFORMATION

Corresponding Author

*E-mail: jhcho94@skku.edu (J.H.C.); bongsoo@kist.re.kr (B.K.).

Author Contributions

⊗These authors equally contributed to this work.

Notes

The authors declare no competing financial interest.

■ ACKNOWLEDGMENTS

This work was supported by the Pioneer Research Center Program (2009-0081500) and Basic Science Research Program (2009-0083540 and 2010-0026294) through the National Research Foundation of Korea funded by the Ministry of Education, Science and Technology. It was also partially supported by the Small Business Technology Innovation Program (S1071663) funded by the SMBA

■ REFERENCES

(1) Facchetti, A. *Chem. Mater.* **2010**, *23*, 733.
(2) Zaumseil, J.; Sirringhaus, H. *Chem. Rev.* **2007**, *107*, 1296.
(3) Zhang, W.; Smith, J.; Watkins, S. E.; Gysel, R.; McGehee, M.; Salleo, A.; Kirkpatrick, J.; Ashraf, S.; Anthopoulos, T.; Heeney, M.; McCulloch, I. *J. Am. Chem. Soc.* **2010**, *132*, 11437.
(4) Tsao, H. N.; Cho, D.; Andreasen, J. W.; Rouhanipour, A.; Breiby, D. W.; Pisula, W.; Müllen, K. *Adv. Mater.* **2009**, *21*, 209.
(5) He, M.; Li, J.; Sorensen, M. L.; Zhang, F.; Hancock, R. R.; Fong, H. H.; Pozdin, V. A.; Smilgies, D.-M.; Malliaras, G. G. *J. Am. Chem. Soc.* **2009**, *131*, 11930.
(6) Kim, D. H.; Lee, B.-L.; Moon, H.; Kang, H. M.; Jeong, E. J.; Park, J.-I.; Han, K.-M.; Lee, S.; Yoo, B. W.; Koo, B. W.; Kim, J. Y.; Lee, W. H.; Cho, K.; Becerril, H. A.; Bao, Z. *J. Am. Chem. Soc.* **2009**, *131*, 6124.
(7) Bao, Z.; Dodabalapur, A.; Lovinger, A. J. *Appl. Phys. Lett.* **1996**, *69*, 4108.
(8) Ong, B. S.; Wu, Y.; Liu, P.; Gardner, S. *J. Am. Chem. Soc.* **2004**, *126*, 3378.
(9) McCulloch, I.; Heeney, M.; Bailey, C.; Genevicius, K.; I, M.; Shkunov, M.; Sparrowe, D.; Tierney, S.; Wagner, R.; Zhang, W. M.; Chabinyc, M. L.; Kline, R. J.; Mcgehee, M. D.; Toney, M. F. *Nat. Mater.* **2006**, *5*, 328.
(10) Li, Y.; Sonar, P.; Singh, S. P.; Soh, M. S.; van Meurs, M.; Tan, J. *J. Am. Chem. Soc.* **2011**, *133*, 2198.
(11) Ha, J. S.; Kim, K. H.; Choi, D. H. *J. Am. Chem. Soc.* **2011**, *133*, 10364.
(12) Li, Y.; Singh, S. P.; Sonar, P. *Adv. Mater.* **2010**, *22*, 4862.
(13) Usta, H.; Facchetti, A.; Marks, T. J. *Acc. Chem. Res.* **2011**, *44*, 501.
(14) Lee, J.-K.; Gwinner, M. C.; Berger, R.; Newby, C.; Zentel, R.; Friend, R. H.; Sirringhaus, H.; Ober, C. K. *J. Am. Chem. Soc.* **2011**, *133*, 9949.
(15) Newman, C. R.; Frisbie, C. D.; da Silva Filho, D. A.; Brédas, J.-L.; Ewbank, P. C.; Mann, K. R. *Chem. Mater.* **2004**, *16*, 4436.
(16) Babel, A.; Jenekhe, S. A. *Synth. Met.* **2005**, *148*, 169.
(17) Usta, H.; Risko, C.; Wang, Z.; Huang, H.; Deliomeroglu, M. K.; Zhukhovitskiy, A.; Facchetti, A.; Marks, T. J. *J. Am. Chem. Soc.* **2009**, *131*, 5586.
(18) Letizia, J. A.; Salata, M. R.; Tribout, C. M.; Facchetti, A.; Ratner, M. A.; Marks, T. J. *J. Am. Chem. Soc.* **2008**, *130*, 9679.
(19) Chen, Z.; Zheng, Y.; Yan, H.; Facchetti, A. *J. Am. Chem. Soc.* **2008**, *131*, 8.
(20) Zhan, X.; Tan, Z. A.; Domercq, B.; An, Z.; Zhang, X.; Barlow, S.; Li, Y.; Zhu, D.; Kippelen, B.; Marder, S. R. *J. Am. Chem. Soc.* **2007**, *129*, 7246.

(21) Oh, J. H.; Suraru, S. L.; Lee, W.-Y.; Könemann, M.; Höffken, H. W.; Röger, C.; Schmidt, R.; Chung, Y.; Chen, W.-C.; Würthner, F.; Bao, Z. *Adv. Funct. Mater.* **2010**, *20*, 2148.
(22) Schmidt, R. D.; Oh, J. H.; Sun, Y.-S.; Deppisch, M.; Krause, A.-M.; Radacki, K.; Braunschweig, H.; Könemann, M.; Erk, P.; Bao, Z.; Würthner, F. *J. Am. Chem. Soc.* **2009**, *131*, 6215.
(23) Yan, H.; Chen, Z.; Zheng, Y.; Newman, C.; Quinn, J. R.; Dotz, F.; Kastler, M.; Facchetti, A. *Nature* **2009**, *457*, 679.
(24) Crone, B.; Dodabalapur, A.; Lin, Y. Y.; Filas, R. W.; Bao, Z.; LaDuca, A.; Sarpeshkar, R.; Katz, H. E.; Li, W. *Nature* **2000**, *403*, 521.
(25) Meijer, E. J.; de Leeuw, D. M.; Setayesh, S.; van Veenendaal, E.; Huisman, B. H.; Blom, P. W. M.; Hummelen, J. C.; Scherf, U.; Klapwijk, T. M. *Nat. Mater.* **2003**, *2*, 678.
(26) Smith, J.; Bashir, A.; Adamopoulos, G.; Anthony, J. E.; Bradley, D. D. C.; Heeney, M.; McCulloch, I.; Anthopoulos, T. D. *Adv. Mater.* **2010**, *22*, 3598.
(27) Xia, Y.; Zhang, W.; Ha, M.; Cho, J. H.; Renn, M. J.; Kim, C. H.; Frisbie, C. D. *Adv. Funct. Mater.* **2010**, *20*, 587.
(28) Ha, M.; Xia, Y.; Green, A. A.; Zhang, W.; Renn, M. J.; Kim, C. H.; Hersam, M. C.; Frisbie, C. D. *ACS Nano* **2010**, *4*, 4388.
(29) Kim, F. S.; Guo, X.; Watson, M. D.; Jenekhe, S. A. *Adv. Mater.* **2010**, *22*, 478.
(30) Sonar, P.; Singh, S. P.; Li, Y.; Soh, M. S.; Dodabalapur, A. *Adv. Mater.* **2010**, *22*, 5409.
(31) Bürgi, L.; Turbiez, M.; Pfeiffer, R.; Bienewald, F.; Kirner, H.-J.; Winnewisser, C. *Adv. Mater.* **2008**, *20*, 2217.
(32) Bijleveld, J. C.; Zoombelt, A. P.; Mathijssen, S. G. J.; Wienk, M. M.; Turbiez, M.; de Leeuw, D. M.; Janssen, R. A. J. *J. Am. Chem. Soc.* **2009**, *131*, 16616.
(33) Bronstein, H.; Chen, Z.; Ashraf, R. S.; Zhang, W.; Du, J.; Durrant, J. R.; Shakya Tuladhar, P.; Song, K.; Watkins, S. E.; Geerts, Y.; Wienk, M. M.; Janssen, R. A. J.; Anthopoulos, T.; Sirringhaus, H.; Heeney, M.; McCulloch, I. *J. Am. Chem. Soc.* **2011**, *133*, 3272.
(34) Zhang, W. M.; Smith, J.; Watkins, S. E.; Gysel, R.; McGehee, M.; Salleo, A.; Kirkpatrick, J.; Ashraf, S.; Anthopoulos, T.; Heeney, M.; McCulloch, I. *J. Am. Chem. Soc.* **2010**, *132*, 11437.
(35) Najari, A.; Beaupré, S.; Berrouard, P.; Zou, Y.; Pouliot, J.-R.; Lepage-Pérusse, C.; Leclerc, M. *Adv. Funct. Mater.* **2011**, *21*, 718.
(36) Yiu, A. T.; Beaujuge, P. M.; Lee, O. P.; Woo, C. H.; Toney, M. F.; Fréchet, J. M. J. *J. Am. Chem. Soc.* **2011**, *134*, 2180.
(37) Woo, C. H.; Beaujuge, P. M.; Holcombe, T. W.; Lee, O. P.; Fréchet, J. M. J. *J. Am. Chem. Soc.* **2010**, *132*, 15547.
(38) Li, Z.; Tsang, S.-W.; Du, X.; Scoles, L.; Robertson, G.; Zhang, Y.; Toll, F.; Tao, Y.; Lu, J.; Ding, J. *Adv. Funct. Mater.* **2011**, *21*, 3331.
(39) Kline, R. J.; DeLongchamp, D. M.; Fischer, D. A.; Lin, E. K.; Richter, L. J.; Chabinyc, M. L.; Toney, M. F.; Heeney, M.; McCulloch, I. *Macromolecules* **2007**, *40*, 7960.
(40) Causin, V.; Marega, C.; Marigo, A.; Valentini, L.; Kenny, J. M. *Macromolecules* **2004**, *38*, 409.
(41) Malik, S.; Nandi, A. K. *J. Polym. Sci., Part B: Polym. Phys.* **2002**, *40*, 2073.